Eur. Phys. J. A **12**, 387–397 (2001)

THE EUROPEAN PHYSICAL JOURNAL A

Investigation of inelastic α-scattering on ^{24}Mg and ^{28}Si

A.K. Basak[1,a], M.N.A. Abdullah[1], A.S.B. Tariq[1], S.K. Das[1,2], A.F.M.M. Rahman[1], A.S. Mondal[1], H.M. Sen Gupta[3], and F.B. Malik[4]

[1] Department of Physics, University of Rajshahi, Rajshahi, Bangladesh
[2] Department of Physics, Shahjalal University of Science & Technology, Sylhet, Bangladesh
[3] Department of Physics, University of Dhaka, Dhaka, Bangladesh
[4] Department of Physics, Southern Illinois University, Carbondale, IL 62901, U.S.A.

Received: 25 September 2001 / Revised version: 21 November 2001
Communicated by W.F. Henning

Abstract. Effects of three different α-nucleus potentials, the normal Woods-Saxon (WS), the squared WS and the molecular, have been studied using the differential cross-section data of inelastically scattered α-particles on ^{24}Mg and ^{28}Si at 54 and 26 MeV incident energies, respectively. The angular distributions of inelastic scattering to the first 2^+ and 4^+ states of the two nuclei have been analyzed in terms of a coupled-channel formalism. The macroscopic rotational model using both the squared WS and the molecular potentials can produce satisfactorily a simultaneous description of the elastic data and the inelastic-scattering data of the 2^+ and 4^+ states for both the targets. The normal WS potential fails to describe the elastic and inelastic data, simultaneously. The effects of second-order deformed potential are also investigated. Microscopic coupled-channel calculations, using the 0^+-2^+ coupling and the Gaussian α-nucleon interaction in the form-factor, have also been performed for the ^{28}Si target using both the squared WS and molecular potentials, the latter one giving a reasonable description of the data.

PACS. 24.10.Eq Coupled-channel and distorted-wave models

1 Introduction

In an effort to determine the nature of α-light nucleus interaction, we have analyzed the elastic scattering of α-particles by ^{28}Si and ^{24}Mg [1] and particle transfer reactions, ^{27}Al$(\alpha,\mathrm{t})^{28}$Si [2,3], ^{28}Si$(\alpha,\mathrm{d})^{30}$P [4,5] and ^{28}Si$(\alpha,\mathrm{p})^{31}$P [6]. The data on the elastic scattering of α-particles by ^{28}Si and ^{24}Mg, exhibiting large enhancement at backward angles known as anomalous large-angle scattering (ALAS), are well described by two simple local potentials. One is due to Michel and his collaborators [7–10], which has a squared Woods-Saxon (WS) form and is referred to as the Michel potential and the other is due to Malik and his collaborators [11–14], which has a non-monotonic real part with a short-range repulsion and is referred to as the molecular potential. The data on the above-mentioned (α,d) and (α,p) transfer reactions [4,6] are, however, better accounted for by the molecular potential. In the light of that, it is of interest to investigate the extent to which these two potentials can account for the available data on inelastic scattering of α-particles by ^{24}Mg and ^{28}Si. For this purpose it is important to select data having large angular distribution at a fixed energy for both elastic and inelastic scattering. Such data exist for elastic and inelastic scattering of α-particles by ^{28}Si and ^{24}Mg at 26 and 54 MeV incident energies, respectively, leading to their ground (elastic) and first 2^+ and 4^+ states. The data for ^{28}Si exhibit prominently the ALAS behavior and those in the case of ^{24}Mg, at the incident energy considered, exhibit a pattern similar to ALAS but far from the one expected of a rainbow scattering [15]. So far to the best of our knowledge, no attempt has been made to analyze the inelastic data for ^{28}Si. Efforts to fit the data for ^{24}Mg by the standard WS and the folding potentials have met with limited success [16,17]. In particular the fits to elastic-scattering data in [16,17] for 42 and 50 MeV incident energies are not as good as those done using the molecular and Michel potentials [1]. It is, therefore, important to examine whether the latter two potentials could account for these data.

We adopt the coupled-channel (CC) formalism described in sect. 3 to analyze the data. This requires the knowledge of α-nucleus potential, which is described in sect. 2. In this investigation, the parameters of the potential for coupling between the channels are the same as those used for the elastic channel. However, for the inelastic channels different parameters are allowed to vary in securing satisfactory fits to the data.

[a] e-mail: akbasak2001@yahoo.com

The calculations require knowledge of the structure of the bound states involved. The ground and first 2^+ and 4^+ states of ^{24}Mg are well described by the rotational model [18]. Inelastic scattering to such states can be described by the macroscopic model where the incident α-particle interacts in the surface region of the target nucleus with a deformed α-nucleus potential [19–21]. The impact of the α-nucleus potential manifests in two ways: first, in generating distorted waves in the incident and final channels and second, in determining the nature of the deformed potential for the form-factor responsible for the transition to the final state.

The low-lying energy spectra of ^{24}Mg and ^{28}Si are well described in the shell model with configuration interaction used by Wildenthal and McGrory [22]. However, as noted by them, the explanation of electric quadrupole transition rates requires the use of effective charge of both neutrons and protons. This enhancement could be construed as an embodiment of the collective character of these states. We, therefore, computed the inelastic cross-sections using both macroscopic and microscopic pictures. The latter is, however, restricted to the 2^+ state of ^{28}Si only. The formalism for macroscopic and microscopic calculations are noted in sects. 3 and 4, respectively. Section 5 provides the details of the analysis. Section 6 contains the discussion. The conclusions are drawn in the subsequent section.

2 Choice of α-nucleus potentials

The Michel potential [7–10] including the Coulomb term $V_C(r)$ comprises of the following forms of the real, $V_M(r)$ and imaginary, $W_M(r)$ parts:

$$V_M(r) = -V_0\left[1+\alpha\exp\left\{-\left(\frac{r}{\rho}\right)^2\right\}\right] \times\left[1+\exp\left(\frac{r-R_R}{2a_R}\right)\right]^{-2} + V_C(r)\,, \quad (1)$$

$$W_M(r) = -W_0\left[1+\exp\left(\frac{r-R_W}{2a_W}\right)\right]^{-2}, \quad (2)$$

with

$$V_C(r) = \left[\frac{Z_1Z_2e^2}{2R_C}\right]\left[3-\frac{r^2}{R_C^2}\right] \text{ for } r\le R_C = \frac{Z_1Z_2e^2}{r} \text{ for } r>R_C. \quad (3)$$

Here $R_i = r_iA_T^{1/3}$ (i = R, W, C), and A_T is the target-mass number.

The molecular potential, which is obtained from a many-body theory utilizing the energy density functional method [11–13], has the following forms for the real, $V_m(r)$ and imaginary, $W_m(r)$ parts:

$$V_m(r) = -V_0\left[1+\exp\left(\frac{r-R_R}{a_R}\right)\right]^{-1} +V_1\exp\left[-\left(\frac{r}{R_1}\right)^2\right] + V_C(r)\,, \quad (4)$$

$$W_m(r) = -W_0\exp\left[-\left(\frac{r}{R_W}\right)^2\right]. \quad (5)$$

The Coulomb potential $V_C(r)$ is given by (3). The real part is non-monotonic with a short-range repulsion. R_C in the molecular potential is the sum of the radii of an α-particle and the target nucleus and not equal to $r_CA_T^{1/3}$. The parameters R_R, R_1, R_W and R_C could sometimes be scaled among neighboring nuclei [1,13] by $R_i = R_{\alpha i} + r_0A_T^{1/3}$ ($i = R, 1, W, C$) with $r_0 = 1.35$ fm.

The standard deep and shallow WS potential for the α-nucleus system including the Coulomb term in (3) is given by

$$V(r) = V_C(r) - Vf(x_R) - iWf(x_W), \quad (6)$$

where, $f(x_i) = (1+e^{x_i})^{-1}$ with $x_i = \left(r - r_iA_T^{1/3}\right)/a_i$ ($i = R, W$).

3 Formalism of second-order effect in macroscopic model

The transition matrix element [23,24] for an inelastic scattering is given by

$$T_{fi}(\mathbf{k}',\mathbf{k}) = \int \mathrm{d}^3\mathbf{r}\chi_f^{-*}(\mathbf{k}',\mathbf{r})\langle\Phi_f|V(\mathbf{r},\xi)|\Phi_i\rangle\chi_f^{+}(\mathbf{k},\mathbf{r}), \quad (7)$$

where χ^+ and χ^-, the distorted waves in the incident and outgoing channels are the approximate solutions of CC equations involving the channels in consideration but omitting the off-diagonal terms. Φ_i and Φ_f are, respectively, the target nuclear wave functions in the initial and final channels coupled through the nucleon-nucleus interaction $V(\mathbf{r},\xi)$ having the multipole expansion [24]:

$$V(\mathbf{r},\xi) = \sum_{JM} V_{JM}(r,\xi)\left[i^JY_{JM}\right]^*. \quad (8)$$

Here ξ represents the internal coordinates of the target nucleus. The matrix element of interaction between the initial i and final f states, after using the Wigner-Eckart theorem, is given by

$$V_{fi} = \langle\Phi_f|V(\mathbf{r},\xi)|\Phi_i\rangle = \sum_{JM}(J_iM_iJM \mid J_fM_f) \times\langle\Phi_f \parallel V_J \parallel \Phi_i\rangle\left[i^JY_{JM}(\hat{r})\right]^*. \quad (9)$$

The form-factor for the transfer of angular momentum J is given by

$$A_J F_J(r) = \int \Phi_f^*(\xi)\, V_J(r,\xi)\, \Phi_i(\xi)\, \mathrm{d}^3\xi = \langle \Phi_f \parallel V_J \parallel \Phi_i \rangle = V_{fi}^{JM} / \left\{ \left[i^J Y_{JM}(\mathbf{r}) \right]^* \times (J_i M_i JM \mid J_f M_f) \right\}. \quad (10)$$

In (10) V_{fi}^{JM} represents the matrix element of interaction responsible for the J-transfer in an inelastic scattering. In the rotational model, the deformation δR of a nucleus with axial symmetry can be defined [24] in terms of the usual deformation parameter β_k as

$$\delta R = R - R_0 = R_0 \sum_{k\nu} \beta_k Y_{k\nu}^*(\mathbf{r}) D_{\nu 0}^k(\hat{s}). \quad (11)$$

Here $\hat{s}$ denotes the Euler angles of the body-fixed frame with respect to the space-fixed frame, $\hat{r}$ defines the angles for the scattering and R_0 is the radius of the spherical nucleus. Equation (11) leads to

$$(\delta R)^2 = 2R_0^2 \sum_{JM} \beta_{2\mathrm{nd}}^{(J)} D_{M0}^J(\hat{s}) Y_{JM}^*(\hat{r}), \quad (12)$$

where

$$\beta_{2\mathrm{nd}}^{(J)} = \frac{1}{2\sqrt{4\pi}} \sum_{kk'} \beta_k \beta_k' \frac{\hat{k}\hat{k'}}{\hat{J}}, \text{ with } \hat{k} = (2k+1)^{1/2}. \quad (13)$$

The macroscopic form-factor as defined in (10) depends on the geometry of the interaction potential, since it involves the expansion of the potential in a Taylor series around the nuclear radius R_0. Writing $V(r,R) = V_0 f(r-R)$, one may expand $f(r-R)$ as

$$f(r-R) = f(r-R_0) - \delta R \frac{\mathrm{d}}{\mathrm{d}r} f(r-R_0) + \frac{1}{2}(\delta R)^2 \frac{\mathrm{d}^2}{\mathrm{d}r^2} f(r-R_0), \quad (14)$$

where R is the deformed radius with the deformation δR defined in (11). Thus, the first- and second-order form-factors are, respectively, given by

$$A_J^{(1)} F_J^{(1)} = \frac{-i^J \beta_J R_0 V_0 \frac{\mathrm{d}f}{\mathrm{d}r} \left\langle J_f M_f K \mid D_{M0}^J \mid J_i M_i K \right\rangle}{(J_i M_i JM \mid J_f M_f)}, \quad (15)$$

and

$$A_J^{(2)} F_J^{(2)} = \frac{i^J \beta_{2\mathrm{nd}}^{(J)} R_0^2 V_0 \frac{\mathrm{d}^2 f}{\mathrm{d}r^2} \left\langle J_f M_f K \mid D_{M0}^J \mid J_i M_i K \right\rangle}{(J_i M_i JM \mid J_f M_f)}. \quad (16)$$

In (15) and (16), the initial and final nuclear wave functions belong to the same rotational band K. Using the nuclear wave functions [25] for an axially symmetric rotor,

$$|JMK\rangle = \left[\frac{(2J+1)}{16\pi^2 (1+\delta_{K0})} \right]^{\frac{1}{2}} \times \left[D_{MK}^J(\hat{s}) + (-1)^J D_{M-K}^J(\hat{s}) \right], \quad (17)$$

one can reduce the above two form-factors for transitions between members of a $K=0$ rotational band to

$$A_J^{(1)} F_J^{(1)}(r) = -i^J \frac{\hat{J}_i}{\hat{J}_f} (J_i 0 J 0 \mid J_f 0) \beta_J \left[V_0 R_0 \frac{\mathrm{d}f}{\mathrm{d}r} \right] \quad (18)$$

and

$$A_J^{(2)} F_J^{(2)}(r) = i^J \frac{\hat{J}_i}{\hat{J}_f} (J_i 0 J 0 \mid J_f 0) \beta_{2\mathrm{nd}}^{(J)} \left[V_0 {R_0}^2 \frac{\mathrm{d}^2 f}{\mathrm{d}r^2} \right]. \quad (19)$$

For a Gaussian interaction, it is customary to expand the deformed Gaussian potential $V_G(r)$ given by

$$V_G(r) = V_0 \exp\left[-\frac{r^2}{R^2} \right], \quad (20)$$

in terms of its spherically symmetric counterpart $V_G^S(r)$ defined by

$$V_G^S(r) = V_0 \exp\left[-\frac{r^2}{R_0^2} \right]. \quad (21)$$

To achieve this, one may use the following notations:

$$x = -\frac{r^2}{R_0^2} \text{ and } h = \frac{r^2}{R_0^2} - \frac{r^2}{R^2}. \quad (22)$$

In terms of the deformation δR, one can write

$$h = \frac{r^2}{R_0^2} \left[2\frac{\delta R}{R_0} - 3\left(\frac{\delta R}{R_0} \right)^2 \right]. \quad (23)$$

The interaction potential in (20) can be expanded up to the second-order term of the Taylor series as

$$V_G(r) = V_0 \exp x + h V_0 \frac{\mathrm{d}}{\mathrm{d}x} \exp x + \frac{h^2}{2} V_0 \frac{\mathrm{d}^2}{\mathrm{d}x^2} \exp x = V_G^S(r) + \frac{r^2}{R_0^2} \left[2\frac{\delta R}{R_0} - 3\left(\frac{\delta R}{R_0} \right)^2 \right] V_G^S(r) + \frac{1}{2} \frac{r^4}{R_0^4} \left[2\frac{\delta R}{R_0} - 3\left(\frac{\delta R}{R_0} \right)^2 \right]^2 V_G^S(r). \quad (24)$$

The first- and second-order interaction potentials responsible for the inelastic scattering can be obtained by collecting the terms in δR and $(\delta R)^2$, respectively, from (24). Denoting these, respectively, by $V^{(1)}$ and $V^{(2)}$, one obtains

$$V^{(1)}(r) = \frac{2}{R_0^2} r^2 \frac{\delta R}{R_0} V_G^S(r) \quad (25)$$

and

$$V^{(2)}(r) = \frac{1}{2} \left[\left(\frac{2}{R_0^2} \right)^2 r^4 - 3\left(\frac{2}{R_0^2} \right) r^2 \right] \left[\frac{\delta R}{R_0} \right]^2 V_G^S(r). \quad (26)$$

These lead to the following first- and second-order form-factors for transitions between members of a $K=0$ rotational band in case of Gaussian interaction, respectively, as

$$A_J^{(1)} F_J^{(1)}(r) = i^J \frac{\hat{J}_i}{\hat{J}_f} (J_i 0 J 0 \mid J_f 0) \beta_J \left[\frac{2}{R_0^2} r^2 V_G^S(r) \right] \quad (27)$$

and

$$A_J^{(2)} F_J^{(2)}(r) = i^J \frac{\hat{J}_i}{\hat{J}_f} (J_i 0 J 0 \mid J_f 0)\, \beta_{2\mathrm{nd}}^{(J)} \times \left[\left(\frac{2}{R_0^2} \right)^2 r^4 - 3 \left(\frac{2}{R_0^2} \right) r^2 \right] V_G^S(r). \quad (28)$$

The strengths $A_J^{(1)}$ and $A_J^{(2)}$ in (18) and (19) or in (27) and (28) can be appropriately partitioned in feeding the potential parameters.

4 Microscopic form-factor

For calculation of microscopic form-factor for the inelastic scattering to the 1.78 MeV (2^+) state of ^{28}Si, the spectroscopic amplitudes are obtained using the wave functions of Wildenthal and McGrory [22]. The spectroscopic amplitude γ, which is the product of the projectile spectroscopic amplitude $s = 4.0$ [26] and the target spectroscopic amplitude S [27], can be written as

$$\gamma(JJ_iJ_f; TT_iT_f; j_1 j_2) = 4S(JJ_iJ_f; TT_iT_f; j_1 j_2), \quad (29)$$

where

$$S(JJ_iJ_f; TT_iT_f; j_1 j_2) = A\hat{J}_i\hat{J}_f\hat{T}_i\hat{T}_f \times \sum_{J_C T_C} W(J_i J_C J j_2; j_1 J_f)\, W\left(T_i T_C T \frac{1}{2}; \frac{1}{2} T_f\right) \times \sum_{mn} a_i^m a_f^n I_i^m I_f^n. \quad (30)$$

Here $(J_i; T_i)$, $(J_f; T_f)$ and $(J_C; T_C)$ are, respectively, the spin-isospin configurations of the target, final and core nuclei. j_1 and j_2 refer to the initial and final orbits of the excited nucleon. a's denote the amplitude in the different terms of the shell model wave function in the initial and final nuclei.

In (30), I_i^m and I_f^n [28] are the overlap integrals $\left\langle J_i T_i \mid J_C T_C; j_1 \frac{1}{2} \right\rangle_m$ and $\left\langle J_f T_f \mid J_C T_C; J_2 \frac{1}{2} \right\rangle_n$ for the target and final nucleus corresponding the m-th and n-th configurations in the wave functions. For the model space of the $d_{5/2}$, $s_{1/2}$ and $d_{3/2}$ shell model orbits, I_i^m and I_f^n are calculated from the formulas given in the appendix of [29] using the table of coefficients of fractional parentage in [30].

5 Analysis

CC calculations have been performed using the computer code CHUCK3 [33]. The experimental angular distributions of cross-section for the elastic scattering by ^{28}Si and inelastic scattering to its first 2^+ and 4^+ states are taken from [32,31]. The angular distribution data for the elastic and inelastic scattering by ^{24}Mg are taken from [16,17]. The code has been modified to incorporate the Michel and molecular potentials both for obtaining the distorted waves and for calculating the macroscopic form-factors in the rotational model. The coupling schemes for both the ^{24}Mg and ^{28}Si targets, which are shown as insets in figs. 1-3, couple the 0^+, 2^+ and 4^+ states. The calculations involve the 0^+-2^+ coupling via the quadrupole deformation β_2, the 0^+-4^+ coupling via the hexadecapole deformation β_4 and the 2^+-4^+ coupling via the quadrupole and hexadecapole deformations. The effect of β_6 has been found be very negligible and it is not considered in the present analysis.

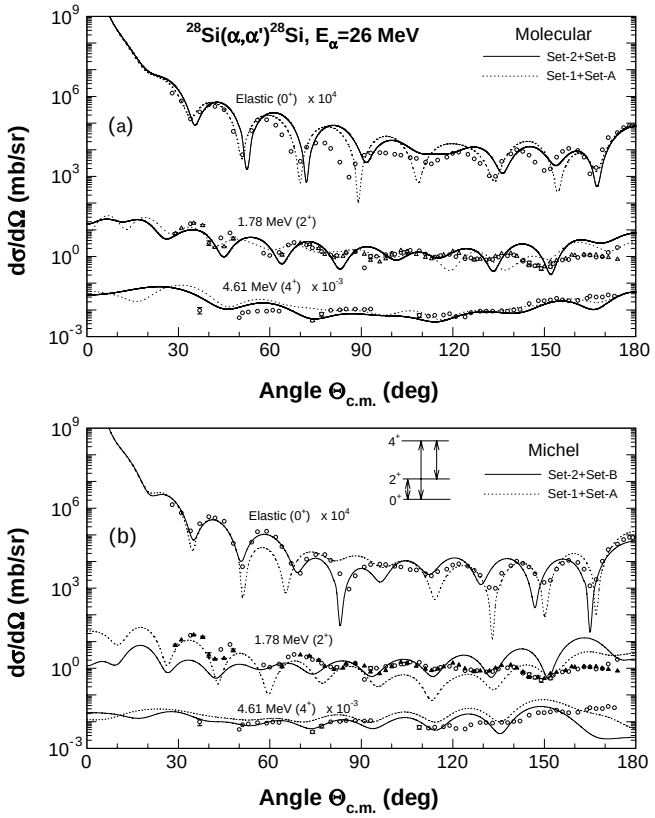

Fig. 1. Comparison of CC macroscopic calculations for the elastic and inelastic α-scattering to the 2^+ and 4^+ states of ^{28}Si to the angular distribution data. The solid curves are the predictions of the potential set-2 using the deformation parameter set-B of table 1 with (a) molecular and (b) Michel potential in the α channel. The coupling scheme is shown in (b). The open circles and the triangles are the experimental points taken, respectively, from [31] and [32].

Table 1. Deformation parameters.

Nucleus	Set	Deformation parameters			
		β_2	β_4	$\beta_{2\mathrm{nd}}^{(2)}$	$\beta_{2\mathrm{nd}}^{(4)}$
^{24}Mg	A	+0.19	−0.05	+0.0114	+0.0039
	B	−0.24	+0.09	+0.0182	+0.0067
^{28}Si	A	+0.18	−0.09	+0.0102	+0.0025
	B	−0.18	+0.10	+0.0102	+0.0024

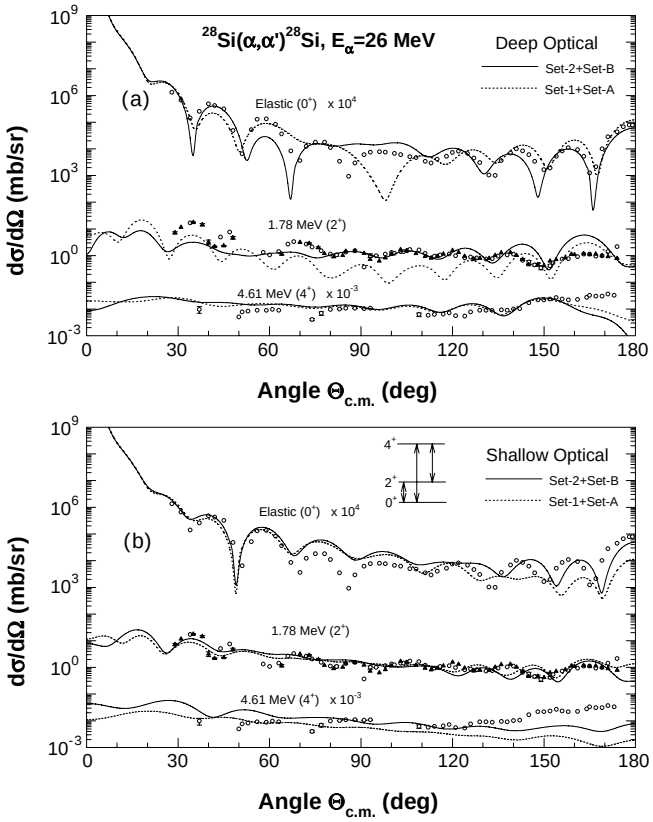

Fig. 2. The same as in fig. 1 with (a) deep and (b) shallow optical (WS) potential in the α channel.

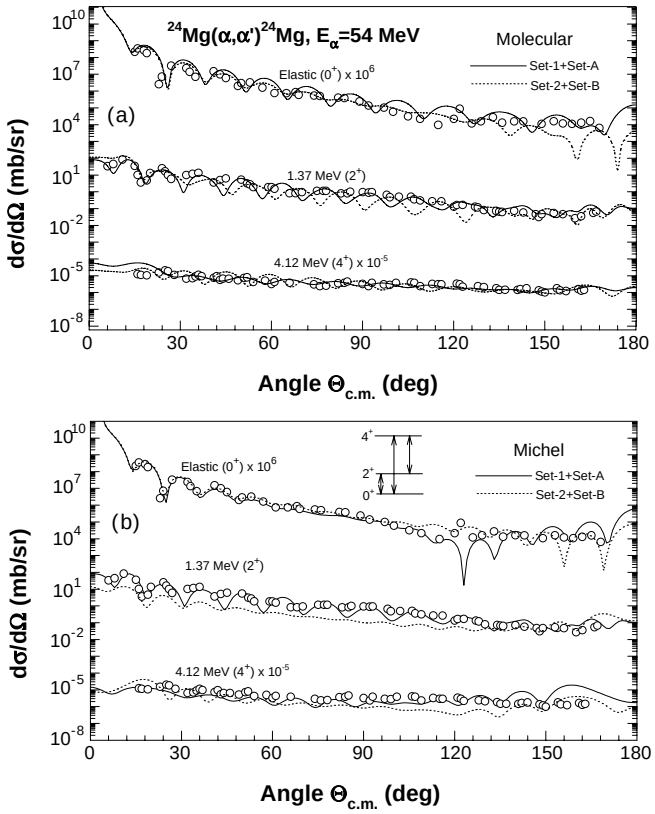

Fig. 3. The same as in fig. 1 but for scattering on ^{24}Mg. The solid and dotted curves are respectively, for set-1 + set-A and set-2 + set-B. The data are from [16,17].

The analysis aiming to obtain the best fit to the experimental angular distributions of cross-section simultaneously for the elastic scattering and the inelastic scattering to the 2^+ and 4^+ states may be summarized as follows:

i) The initial values of the parameters for the molecular and Michel potentials for the α-^{28}Si and α-^{24}Mg systems are taken from Tariq *et al.* [1] and for the deep and shallow WS potentials for the α-^{28}Si scattering from Das *et al.* [6] for the macroscopic as well as microscopic analysis. These are then adjusted to obtain the best fit to the data as noted in ii), iii) and iv) below.

ii) In the macroscopic analyses, all combinations of relative signs of the deformation parameters β_2 and β_4 have been tried and their magnitudes have been varied to obtain a simultaneous best fit to the data of the three 0^+, 2^+ and 4^+ coupled states. The magnitudes and signs of the second-order amplitudes, $\beta^{(2)}_{\rm 2nd}$ and $\beta^{(4)}_{\rm 2nd}$ in (13), however, depend on the deformation parameters β_2 and β_4. The best fit values of the deformation parameters are listed in table 1. The potential parameters for the best overall fits to the elastic and inelastic data are listed in tables 2 and 3. The potential sets 1 and 2 in table 3 correspond, respectively, to the deformation parameter sets A and B in table 1.

iii) For the macroscopic case, the parameters of the best fit are essentially obtained by changing the range of the imaginary part, R_W for the 0^+ elastic and the 2^+ and 4^+ inelastic channels. R_W is found to decrease with the increase of excitation energy of the final states populated in the inelastic scattering. Furthermore, for the case of the molecular potential, the radius of the repulsive part, R_1, has also to be adjusted to lower values with increasing excitation energy of the final states. Table 2 lists the parameter values which remain fixed for both the potential sets and for the 0^+ elastic as well as the 2^+ and 4^+ inelastic channels. Table 3 displays the parameters which vary for the different channels and sets. The parameters of the potential coupling various channels, $V_{\rm CC'}$, have been kept the same as those of the diagonal potential for the elastic channel.

iv) For the macroscopic calculations, the Coulomb excitation has been included keeping the Coulomb radius R_C to be the same as that used in the distorting channels. The effect of the Coulomb excitation is found to be substantial at the forward angles in the angular distribution for the 2^+ state of both ^{24}Mg and ^{28}Si. The effect has been found to be small for the 4^+ state.

v) The effect of the 2^+-4^+ coupling is studied by switching off the coupling path. The calculations with and without the inclusion of the coupling are compared to the data in figs. 5(a) and 6(a) in the following. To examine the size of the second-order effect, the CC calculations are performed also with and without the inclu-

Table 2. Potential parameters fixed over channels and sets.

Parameter	$\alpha + ^{28}$Si				$\alpha + ^{24}$Mg	
	Molecular	Michel	Shallow WS	Deep WS	Molecular	Michel
V_0 (MeV)	26.0	21.0	55.0	216.0	25.4	25.0
R_R (fm)	5.38	5.00	5.16	3.70	5.15	4.65
a_R (fm)	0.34	(a)	0.505	0.67	0.34	0.60
V_1 (MeV)	42.0	-	-	-	42.0	-
R_1 (fm)	(a)	-	-	-	(a)	-
α	-	6.50	-	-	-	7.00
ρ (fm)	-	6.25	-	-	-	5.85
W_0 (MeV)	14.5	(a)	(a)	(a)	27.5	(a)
R_W (fm)	(a)	(a)	5.16	3.98	(a)	(a)
a_W (fm)	-	0.65	0.505	0.67	-	0.65
R_C (fm)	(a)	(a)	(a)	6.32	9.14	3.75

(a) These parameters have different values according to channel and/or set and are given in table 3.

Table 3. Potential parameters that vary according to channel and/or set.

Target	Potential type	Parameter	Set-1			Set-2		
			0^+	2^+	4^+	0^+	2^+	4^+
^{28}Si	Molecular	R_1 (fm)	2.80	2.60	2.20	2.60	2.60	2.20
		R_W (fm)	3.80	3.40	1.80	3.40	3.40	1.40
		R_C (fm)	9.35	9.35	9.35	6.32	6.32	6.32
	Michel	a_R (fm)	0.63	0.63	0.63	0.60	0.60	0.60
		W_0 (MeV)	26.0	26.0	26.0	26.0	26.0	16.0
		R_W (fm)	3.64	2.88	3.04	3.34	3.19	3.04
		R_C (fm)	6.32	6.32	6.32	3.95	3.95	3.95
	Shallow WS	W_0 (MeV)	5.50	5.50	5.00	6.00	6.00	5.50
		R_C (fm)	3.95	3.95	3.95	6.32	6.32	6.32
	Deep WS	W_0 (MeV)	12.0	12.0	14.0	12.0	10.0	14.0
^{24}Mg	Molecular	R_1 (fm)	2.60	2.60	2.60	2.60	2.60	1.60
		R_W (fm)	3.60	3.50	1.40	3.70	3.40	2.60
	Michel	W_0 (MeV)	128.0	115.0	100.0	128.0	128.0	128.0
		R_W (fm)	3.40	3.17	1.87	3.40	3.17	1.87

sion of the second order amplitudes, $\beta^{(2)}_{2\mathrm{nd}}$ and $\beta^{(4)}_{2\mathrm{nd}}$, noted in table 1. The predictions from the calculations with and without the second-order amplitudes are shown in figs. 5(b) and 6(b).

vi) The microscopic calculations for the inelastic scattering are done only to the 2^+ state of ^{28}Si, because of the lack of information on the spectroscopic amplitude on the 4^+ state. The calculations have been carried out using the 0^+-2^+ coupling and using an α-nucleon interaction of Gaussian shape in the form-factor. The subroutines concerning the microscopic form-factor calculations have been taken from Comfort's version of CHUCK3 [26]. The parameters of the Gaussian potential $V_G(r) = -V_0 \exp\left(-K^2 r^2\right)$, have been taken from the work of Ali *et al.* [34] as $V_0 = 47.32$ MeV and $K^2 = 0.17$ fm^{-2}. The spectroscopic amplitudes γ, for transition to the first 2^+ state of ^{28}Si for different core configurations and the allowed j_1 and j_2 orbitals, have been calculated from the wave functions of Wildenthal and McGrory [22] using eqs. (29) and (30) and are listed in table 4. The predictions from the microscopic CC calculations for the elastic scattering from the ground state and inelastic scattering to the 2^+ state, using the molecular and Michel α-^{28}Si potentials, have been compared to the data in fig. 4. The depth and/or radius parameters for the imaginary part of the distorting potential have been adjusted to achieve the optimum fits to the elastic and inelastic data simultaneously. These and the Coulomb radius R_C used in the final calculations are displayed in table 5.

6 Discussion

The best fits to the elastic and inelastic data for the 26 MeV α-particles incident on the ^{28}Si target are shown in fig. 1(a) for the molecular and fig. 1(b) for the Michel potential, while those for the deep and shallow WS potentials are shown in figs. 2(a) and 2(b), respectively. The

Table 4. Spectroscopic amplitudes for microscopic calculations.

Nucleus	E_x(MeV)	J_f^π; T_f	J_C^π; T_C	j_1	j_2	S	$\gamma^{(a)}$
^{28}Si	1.78	2^+; 0	$5/2^+$; 1/2	5/2	5/2	+0.1161	+0.4645
			$5/2^+$; 1/2	5/2	1/2	−0.1030	−0.4119
			$1/2^+$; 1/2	1/2	5/2	+0.0105	+0.0420
			$1/2^+$; 1/2	1/2	3/2	−0.0590	−0.2360
			$3/2^+$; 1/2	3/2	1/2	+0.0039	+0.0156

$^{(a)}\gamma = 4.0S$ is the spectroscopic strength.

Table 5. α-^{28}Si potential parameters adjusted for microscopic calculations.

Parameter	Molecular		Michel	
	g.s. (0^+)	1.78 MeV (2^+)	g.s. (0^+)	1.78 MeV (2^+)
a_R (fm)	0.37	0.37	0.60	0.60
W_0 (MeV)	14.5	14.5	33.0	12.0
R_W (fm)	3.80	2.80	3.64	3.04
R_C (fm)	6.32	6.32	3.95	3.95

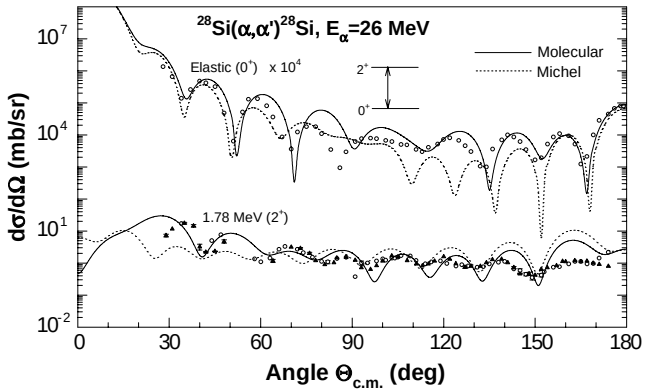

Fig. 4. Comparison of CC microscopic calculations for the elastic and inelastic scattering to the 2^+ state of ^{28}Si with the data. The solid and dotted curves are, respectively, for the molecular and Michel potentials.

coupling scheme is shown in inserts of figs. 1 and 2. All calculations involve this coupling scheme and the deformation parameters including the second-order $\beta_{2\text{nd}}^{(2)}$ and $\beta_{2\text{nd}}^{(4)}$ amplitudes as noted in table 1. (Set-1 + set-A) and (set-2 + set-B) in each of the figures refer to the potential parameter sets 1 and 2 as noted in table 3 along with the deformation parameter sets A and B as noted in table 1. Clearly, both the deep and shallow WS potentials fail to reproduce the data adequately, particularly at large scattering angles (fig. 2). Hence these two potentials are excluded from further discussion.

As can be seen in fig. 1, the calculations using the molecular potential with both (set-1 + set-A) and (set-2 + set-B) reproduce reasonably the angular distributions of the elastic and inelastic scattering to the 4^+ state. However, there is some discrepancy between the data and the calculations for the inelastic scattering to the 2^+ state at very large angles. The calculations using the Michel potential produce a better description of the elastic data for the (set-1 + set-A) and (set-2 + set-B) combinations, but there are discrepancies between the predictions and the data for the inelastic scattering to both the 2^+ and 4^+ states, at large angles. The combination (set-2 + set-B) gives the better overall fits to the elastic and inelastic data for both the molecular and Michel potentials. χ^2-values do not necessarily indicate a measure of quality of fits. Nevertheless, the values of chi-square per point, χ^2/N are presented in table 6 so that these in conjunction with the visual examination of fig. 1 may be useful to the readers in determining the performance of the molecular and Michel potentials.

The values of the deformation parameter β_2 used in set-A for ^{24}Mg and set-B for ^{28}Si (table 1), are in line with those of Malik and Scholz [35] where $\beta_2 = +0.3$ and -0.14 were needed to explain the spectra of the adjacent nuclei ^{25}Mg and ^{29}Si, respectively. But Möller *et al.* [36] require somewhat larger magnitudes, namely, $\beta_2 = +0.374$ and $\beta_4 = -0.053$ for ^{24}Mg and $\beta_2 = -0.478$ and $\beta_4 = +0.250$ for ^{28}Si in order to fit their masses accurately with a liquid-drop–type mass formula.

In fig. 3, the calculations which provide the best fits to the data for the elastic and inelastic scattering to the 2^+ and 4^+ states in ^{24}Mg in the macroscopic approximation using both the potentials are plotted along with the data. The parameters of the potentials for the best fits are noted in table 1. The molecular potential with the (set-1+set-A) combination provides a satisfactory description of the data for the three cases simultaneously. The calculations for the elastic and inelastic scattering to the 4^+ state using the Michel potential have some discrepancies with the data at large angles. The quality of fit to the 2^+ state is about the same for both potentials using (set-1+set-A). The values of χ^2/N for the two types of α-^{24}Mg, and for two combinations of potential and deformation sets are given in table 6.

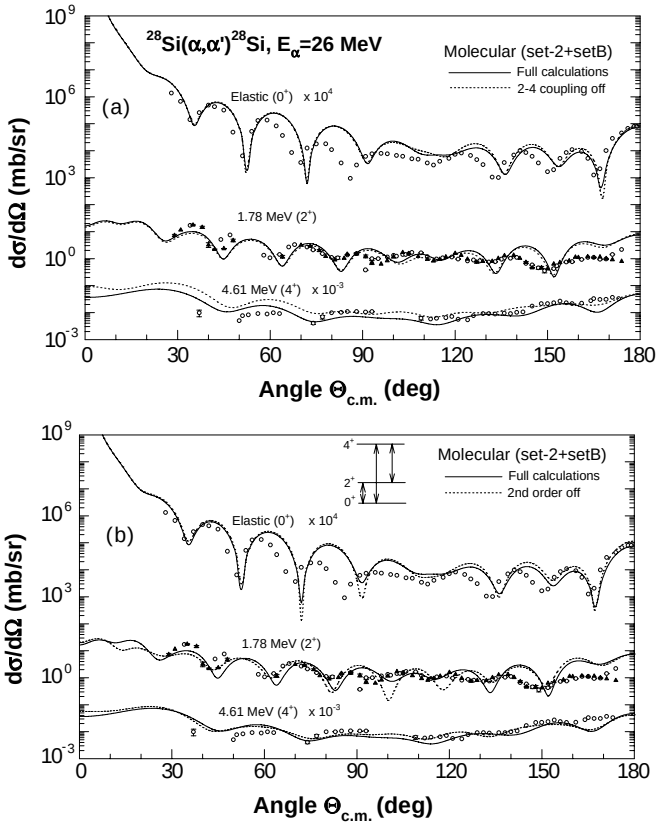

Fig. 5. Comparison of CC macroscopic calculations using the molecular potential set-2 and the deformation parameter set-B to the data of α scattering on ^{28}Si. The solid curves are the predictions from the full calculations and dotted curves are from the calculations without the (a) 2-4 coupling, and (b) second-order deformation amplitudes.

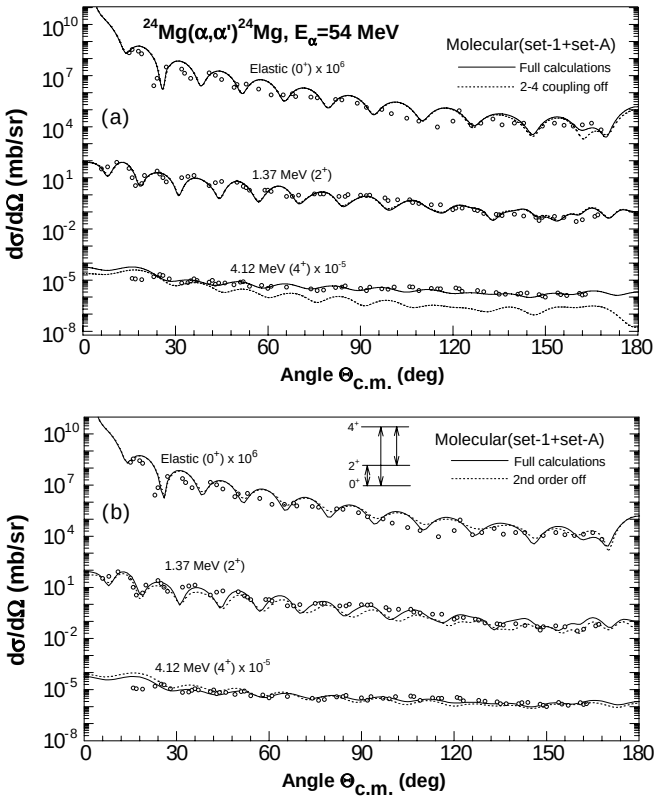

Fig. 6. The same as in fig. 5 for scattering on ^{24}Mg using the molecular potential set-1 and the deformation parameter set-A.

It is interesting to examine the effect of the indirect 2^+-4^+ coupling on the calculations. This is done in figs. 5(a) and 6(a) for the ^{28}Si and ^{24}Mg targets, respectively, using the molecular potential. The effect of its omission is not significant for ^{28}Si, but its inclusion is important for ^{24}Mg, particularly for the inelastic scattering to the 4^+ state. In fact, the good fit to the data for this state could only be obtained once this is included.

The effect of including the second-order amplitudes, $\beta^{(2)}_{\rm 2nd}$ and $\beta^{(4)}_{\rm 2nd}$, on the calculations is shown in figs. 5(b) and 6(b) for the ^{28}Si and ^{24}Mg targets, respectively, using the molecular potential. The inclusion of the second-order terms improves fits to the data of the inelastic scattering to the 2^+ state substantially for both ^{28}Si and ^{24}Mg.

At this stage it is worth to compare the features of the Michel and molecular potentials. The former is a deep monotonic potential and the latter is a shallow non-monotonic one. The real and imaginary parts of the total potential (the sum of the nuclear and Coulomb parts) for both cases are shown in fig. 7. They differ significantly in the interior region, which may be critical to some particle transfer reactions; but are very similar in range and shape near the surface region, which plays prominently in determining the elastic and inelastic scattering in the macroscopic model used here. In this model one expands the potential around the surface to obtain transition matrices responsible for the inelastic scattering. Hence, calculations of the elastic and inelastic scattering using both the potentials reproduce similar results as shown here and in [1], whereas calculations using these two potentials for the (α,d) and (α,p) reactions on ^{28}Si differ significantly [4,6]. It is, thus, necessary to investigate with elastic, inelastic and particle transfer data in order to establish a α-nucleus or nucleus-nucleus interaction, as noted by Satchler [37].

Table 6. Comparative figures of χ^2 per point for best-fit combinations of potential and deformation parameter sets, and the type of α-nucleus potential.

Nucleus	Potential type	Combination of sets	χ^2/N 0^+	2^+	4^+
^{24}Mg	Molecular	Set-1 + set-A	1550	25	36
		Set-2 + set-B	215	85	48
	Michel	Set-1 + set-A	919	21	36
		Set-2 + set-B	178	45	39
^{28}Si	Molecular	Set-1 + set-A	330	34	47
		Set-2 + set-B	1735	106	15
	Michel	Set-1 + set-A	213	52	92
		Set-2 + set-B	64	353	22

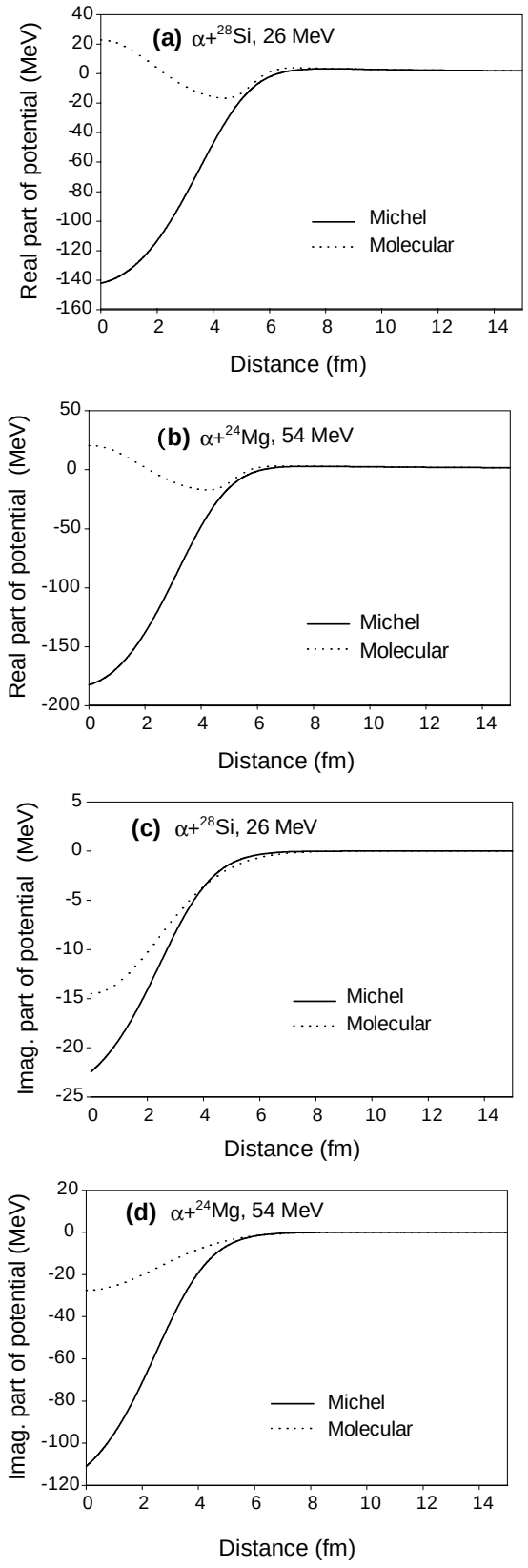

Fig. 7. Comparison of the real and imaginary parts of the molecular ((a) and (c)) and Michel ((b) and (d)) potentials used herein to fit the data for ^{28}Si and ^{24}Mg.

Although the total potentials for the Michel and molecular types are similar in the surface region, the Coulomb radii R_C are quite different for the two cases. In case of the molecular potential, R_C is defined to be that distance between the incident alpha-particle and the target nucleus, beyond which the potential between them is purely the Coulomb type. As noted in [5], parameter values for the real part of the molecular type of α-Si nuclear potential corresponding to $R_C = 1.3A_T^{1/3}$ (as in the Michel potential) are only slightly different to keep the total effective potential same, and give predictions of cross-sections of both the elastic and reaction channels identical to those with the larger R_C used.

The microscopic CC calculations with both the molecular and Michel potentials reproduce the right order of magnitude of cross-sections for the inelastic scattering to the 2^+ state of ^{28}Si. However, only the molecular potential gives satisfactory description of both the elastic and inelastic data, in oscillation and magnitude with the spectroscopic amplitudes noted in table 4.

As noted in Tariq *et al.* [1], the real part of the molecular potential is energy independent over the 14.5–45.0 MeV incident-energy range for ^{28}Si and 22.0–81.0 MeV for ^{24}Mg, while that for the Michel potential for both the targets is dependent on the incident energy through the α-parameter in eq. (1). But the imaginary part is energy dependent for both types of the potentials. The anomalous behaviour in the energy variation of the real part of the central potential and the surface imaginary part of the nucleon-nucleus (near the Fermi energies) [38, 39] and in the α-nucleus (in the energy region 0–50 MeV) [40] optical potential has been well accounted for by invoking the dispersion relations between the real and imaginary parts. In the present work, the correction due to the energy-dependent imaginary part of the optical potential on the real part has been assumed negligible. The results of the present macroscopic analysis on the elastic and inelastic data, on ^{24}Mg in particular, indicate that this is a suitable approximation.

7 Conclusion

The most important conclusion of this investigation along with those of [1–4,6] is that the measurement of a complete angular distribution of differential cross-sections is essential for determining a α-light nucleus potential. ALAS, indeed, is a manifestation of the nature of the potential. Our investigation confirms that the standard WS potential, although may be satisfactory in reproducing the forward-angle data, is inadequate for describing simultaneously the elastic- and inelastic-scattering data over the entire angular range.

The elastic and inelastic data for ^{24}Mg are well accounted for by the molecular potential, particularly when the second-order effects are included in the macroscopic description of the CC analysis. The calculations using the Michel potential fit data adequately but are deficient in the back angles for the inelastic-scattering to the 4^+ state.

The elastic and inelastic scattering data for the ^{28}Si target are reasonably accounted for by the calculations using both potentials but the quality of fits is not as good as the one for ^{24}Mg using the molecular potential. In particular, the inelastic scattering data for the 2^+ and 4^+ states are not very satisfactorily accounted for by both the Michel and molecular potentials. This may arise from the neglect of coupling to the transfer (rearrangement) channels. As noted in [6] that the fits to the angular distributions of cross-sections for the ^{28}Si$(\alpha, \mathrm{p})^{31}$P reaction improve with coupling the reaction channels to the inelastic 2^+ and 4^+ states. The problem may also lie in the wave functions of the 2^+ and 4^+ states of ^{28}Si used here in the macroscopic model. Clearly, the spectrum cannot be described by their being members of a pure $K = 0$ band, as assumed here. Unfortunately, the calculations based on the microscopic model do not improve the fits. In the case of ^{24}Mg, the 2^+ and 4^+ states have large components of the pure $K = 0$ ground-state band which may be the underlying cause for the very good fit.

The CC analyses of the data for the elastic scattering and inelastic scattering to the 2^+ and 4^+ sates of ^{24}Mg in terms of both molecular and Michel potentials clearly indicate that the nucleus is prolate in quadrupole and oblate in hexadecapole deformations. On the other hand, a careful scrutiny of the fits to the elastic and inelastic data in fig. 1, suggests that the ^{28}Si nucleus is oblate in quadrupole and prolate in hexadecapole deformations. However, these deformations are small in magnitude and may be dynamic in nature.

The second-order effects in the macroscopic analyses have been found to be substantial for the inelastic scattering involving the quadrupole transition. In the present work, the inclusion of the second-order effects for the hexadecapole transitions significantly improve the fits to the data, but the total effects arising from the $\beta^{(2)}_{\mathrm{2nd}}$ and $\beta^{(4)}_{\mathrm{2nd}}$ terms are small as the quadrupole and hexadecapole deformation parameters are of opposite signs for both ^{24}Mg and ^{28}Si. But the second-order effects are expected to be large for hexadecapole transitions on a nucleus where β_2 and β_4 are of the same sign.

This work is partly supported by the grant INT-9808892 of the U.S. National Science Foundation and a grant from the ministry of Science and Technology of the Government of Bangladesh. The authors thankfully acknowledge the grants. The authors are also thankful to Professor P.D. Kunz of the University of Colorado for the code CHUCK3 and Professor J.R. Comfort of the Arizona State University for his extended version of CHUCK3. One of the authors, AKB, is thankful to Professor Peter E. Hodgson of Nuclear Physics Laboratory, University of Oxford for encouraging and helping the work by supplying many preprints and reprints of published articles.

References

1. A.S.B. Tariq, A.F.M.M. Rahman, S.K. Das, A.S. Mondal, M.A. Uddin, A.K. Basak, H.M. Sen Gupta, F.B. Malik, Phys. Rev. C **59**, 2558 (1999).
2. S.K. Das, A.S.B. Tariq, A.F.M.M. Rahman, P.K. Roy, M.N. Huda, A.S. Mondal, A.K. Basak, H.M. Sen Gupta, F.B. Malik, Phys. Rev. C **60**, 044617 (1999).
3. S.K. Das, A.S.B. Tariq, A.F.M.M. Rahman, P.K. Roy, M.N. Huda, A.S. Mondal, A.K. Basak, H.M. Sen Gupta, F.B. Malik, Phys. Rev. C **62**, 049802 (2000).
4. S.K. Das, A.S.B. Tariq, M.A. Uddin, A.S. Mondal, A.K. Basak, K.M. Rashid, H.M. Sen Gupta, F.B. Malik, Phys. Rev. C **62**, 054605 (2000).
5. S.K. Das, A.S.B. Tariq, A.F.M.M. Rahman, S. Hossain, A.K. Basak, K.M. Rashid, H.M. Sen Gupta, F.B. Malik, Phys. Rev. C **64**, 034605 (2001).
6. S.K. Das, A.K. Basak, K. Banu, A.S. Mondal, A.S.B. Tariq, A.F.M.M. Rahman, H.M. Sen Gupta, F.B. Malik, Phys. Rev. C **62**, 054606 (2000).
7. Th. Delbar, Gh. Grégoire, G. Paic, R. Ceuleneer, F. Michel, R. Vanderpoorten, R. Budzanowski, H. Dabrowski, L. Friendl, K. Grotowski, S. Micek, R. Planeta, A. Strzalkowski, A. Eberhard, Phys. Rev. C **18**, 1237 (1978).
8. F. Michel, J. Albinski, P. Belery, Th. Delbar, Gh. Grégoire, B. Tasiaux, G. Reidemeister, Phys. Rev. C **28**, 1904 (1983).
9. F. Michel, G. Reidemeister, S. Ohkubo, Phys. Rev. Lett. **57**, 1215 (1986).
10. F. Michel, G. Reidemeister, Y. Kondo, Phys. Rev. C **51**, 3290 (1995).
11. L. Rickertson, B. Block, J.W. Clark, F.B. Malik, Phys. Rev. Lett. **22**, 951 (1969).
12. I. Reichstein, F.B. Malik, Phys. Lett. B **37**, 344 (1971).
13. P. Manngård, M. Brenner, M.M. Alam, I. Reichstein, F.B. Malik, Nucl. Phys. A **504**, 130 (1989).
14. M. Alam, F.B. Malik, Phys. Lett. B **237**, 14 (1990).
15. R. Stock, G. Gaul, R. Santo, M. Bernas, B. Harvey, D. Hendrie, J. Mahoney, J. Sherman, J. Steyaert, M. Zisman, Phys. Rev. C **6**, 1226 (1972).
16. R. Neu, S. Welte, H. Clement, H.J. Hauser, G. Staudt, H. Müther, Phys. Rev. C **39**, 2145 (1989).
17. R. Neu, H. Abele, P.D. Eversheim, F. Hinterberger, H. Oberhummer, H. Jäntsch, Chr. Striebel, G. Staudt, M. Walz, J. Phys. Soc. Jpn., Suppl. **58**, 574 (1989).
18. H. Morinaga, Phys. Rev. **101**, 254 (1956).
19. N.K. Glendenning, M. Veneron, Phys. Rev. **144**, 839 (1966).
20. R.H. Bassel, G.R. Satchler, R.M. Drisco, E. Rost, Phys. Rev. **128**, 2693 (1962).
21. N. Austern, J.S. Blair, Ann. Phys. (N.Y.) **33**, 15 (1965).
22. B.H Wildenthal, J.B. McGrory, Phys. Rev. C **7**, 714 (1973).
23. G.R. Satchler, *Introduction to Nuclear Reactions* (Macmillan, London, 1980).
24. D.F. Jackson, *Nuclear Reactions* (Methuen, London, 1970).
25. M.A. Preston, *Physics of the Nucleus* (Addison-Wesley, London, 1965).
26. J.R. Comfort, Write-up on extended version of computer code CHUCK3, private communication.
27. V.A. Madsen, Nucl. Phys. **80**, 177 (1966).
28. P.J. Brussards, P.W. Glaudemans, *Shell-model Applications in Nuclear Spectroscopy* (North-Holland, Amsterdam, 1977).
29. M. Haque, S.K. Das, A.K. Basak, H.M. Sen Gupta, Nuovo Cimento A **111**, 1131 (1998).
30. Shalom Shlomo, Nucl. Phys. A **184**, 545 (1972).

31. A.W. Obst, K.W. Kemper, Phys. Rev. C **6**, 1705 (1972).
32. L. Jarczyk, B. Maciuk, M. Siemaszko, W. Zipper, Acta Phys. Pol. B **7**, 531 (1976).
33. P.D. Kunz, Computer code CHUCK3, private communication.
34. S. Ali, A.A.Z. Ahmad, N. Ferdous, Rev. Mod. Phys. **57**, 923 (1985).
35. F.B. Malik, W. Scholz, in *Nuclear Structure*, edited by A. Hossain *et al.* (North-Holland, Amsterdam, 1967) p. 34.
36. P. Möller, J.R. Nix, W.D. Myers, W.J. Swiatecki, At. Data Nucl. Data Tables **59**, 185 (1995).
37. G.R. Satchler, in *Proceedings of the International Conference on Reactions between Complex Nuclei*, edited by R.L. Robinson *et al.* (North-Holland, Amsterdam, 1974) p. 171.
38. I. Ahmad, W. Haider, J. Phys. G **2** (1976) L157.
39. C. Mahaux, H. Ngo, G.R. Satchler, Nucl. Phys. A **449**, 354 (1986).
40. W. Haider, P.E. Hodgson, Acta Phys. Slov. **44**, 481 (1994).